Comparison of two scanning instruments to measure peripheral refraction in the human eye

Bart Jaeken,[1,*] Juan Tabernero,[1] Frank Schaeffel,[2] and Pablo Artal[1]

[1]*Laboratorio de Optica, Instituto Universitario de Investigación en Óptica y Nanofísica (IUiOyN), Universidad de Murcia, Campus de Espinardo (Edificio 34), 30100 Murcia, Spain*
[2]*Institute for Ophthalmic Research, Section of Neurobiology of the Eye, 72076 Tübingen, Germany*
Corresponding author: bart.jaeken@um.es

To better understand how peripheral refraction affects development of myopia in humans, specialized instruments are fundamental for precise and rapid measurements of refraction over the visual field. We compare here two prototype instruments that measure in a few seconds the peripheral refraction in the eye with high angular resolution over a range of about ±45 deg. One instrument is based on the continuous recording of Hartmann–Shack (HS) images (HS scanner) and the other is based on the photorefraction (PR) principle (PR scanner). On average, good correlations were found between the refraction results provided by the two devices, although it varied across subjects. A detailed statistical analysis of the differences between both instruments was performed based on measurements in 35 young subjects. Both instruments have advantages and disadvantages. The HS scanner also provides the high-order aberration data, while the PR scanner is more compact and has a lower cost. Both instruments are current prototypes, and further optimization is possible to make them even more suitable tools for future visual optics and myopia research and also for different ophthalmic applications.   © 2012 Optical Society of America

OCIS codes: 120.0120, 330.0330.

1. INTRODUCTION

Ever since it was suggested that peripheral refractive error could influence emmetropization [1,2], this hypothesis has received attention [3–5]. More recently, it was shown in rhesus monkeys that spectacle lenses with a hole or a plano zone in the center to permit unobstructed foveal vision while creating a refractive error in the periphery still had large impact on foveal refraction development [6,7]. Ablation of the fovea does not seem to have impact on the change in shape of the eye when myopia is induced by diffusers [8], suggesting that emmetropization in primates may be also controlled by the peripheral retina.

Various studies have shown that there is a difference in peripheral refractions, relative to the fovea, between emmetropic and myopic subjects [2,4,9]. It remains an open question whether the observed differences in peripheral refraction between myopic and emmetropic subjects are causing the eye to grow or are the consequence of eye growth. To unriddle this chicken–egg problem, long-term studies will be necessary, involving many subjects. At least two studies addressed this question [1,10]. In these studies, peripheral refraction was determined by retinoscopy and autorefraction, but only at a few discrete oblique angular positions (6 and 2, respectively). Peripheral refraction data become more reliable when the angular sampling density is higher. If only a few angular positions are sampled, it is hard to fit the shape of the peripheral refraction reliably using a higher-order polynomial. Low sampling density also reduces the chance that local irregularities in eye shape can be detected [11].

Another approach to uncover possible effects of peripheral defocus on the development of foveal myopia involves the use of new spectacle or contact lenses that impose a myopic refraction in the periphery of the visual field. Because studies in animal models have shown that refractive errors imposed by spectacle lenses are compensated by the appropriate changes in eye growth at each position of the visual field [5], it is assumed that myopia progression could be reduced when the focal plane remains in front of the photoreceptor plane, even when this is the case only in the periphery [12,13].

Currently, conventional autorefractors or wavefront sensors are used to measure off-axis refraction by slightly modifying the instrument and asking the subject to look at different fixation points throughout the visual field. Error bars are often large within refractive groups [14,15], and it remains unclear how much of this variability can be attributed to interindividual variability and how much to "noise" of the measurement technique. Turning the eye does not seem to induce significant differences in peripheral refraction and aberrations [16,17]. Nevertheless, the extensive measuring procedure makes it difficult to exclude effects of accommodation when the eye is not cyclopleged. Furthermore, the centration of the instrument with respect to the pupil center off axis was demonstrated to be critical [18]. All these mentioned aspects suggest that developmental studies that are investigating the relationship between off-axis refractive errors and emmetropization are currently limited by a lack of appropriate instrumentation [19].

To overcome these problems by providing more accurate data, new instruments were developed that can scan over the visual field measuring refraction and the optical quality of the eye in terms of higher-order aberrations with high angular resolution. Furthermore, they were optimized to operate fast in the range of a few seconds. Two prototypes of such fast

scanning instruments, the peripheral wavefront sensor [20] and the photoretinoscope [21], are compared in this study.

2. METHODS

The scanning peripheral wavefront sensor is based on the Hartmann–Shack (HS) principle. After the eye is illuminated with an infrared beam, the outcoming wavefront is sampled by a microlens array, placed in conjugation with the pupil plane of the subject, to reconstruct the eye's aberration [22] as an expansion of Zernike polynomials. A detailed description of this instrument is presented elsewhere [20]. To ensure that the microlens array is in a plane conjugate to the subject's pupil plane, the sensor makes a rotational movement with the pupil plane as center. To improve the comfort for the subject and to assure a large pupil size, the instrument uses 780 nm light. The subject's head position is stabilized by means of a head–chin rest. The sensor measures the central 80 deg of visual angle along a horizontal meridian in 1.8 s, taking one HS measurement per degree. A complete series of wavefront aberrations for each degree is obtained. Refraction is then calculated from the retrieved aberration terms.

The principle of the scanning photoretinoscope (PR) is eccentric photorefraction [23]. An arrangement of infrared LEDs (875 nm) that is placed in front of the camera lens generates a bright light spot on the retina. A fraction of this light is reflected and returns through the optics of the eye to the camera. The pupils appear brightly illuminated on a video image that is taken from the face of the subject. The pupil brightness is a function of the position of the LEDs relative to the optical axis of the camera, the refractive error of the subject, and the fundus reflectivity for the infrared light. To be able to determine the sign of the refractive error, the lower part of the camera lens aperture is covered with a shield behind the LEDs, resulting in a brightness gradient in the vertical pupil meridian. This gradient is positive for a hyperopic eye (more light in the top of the pupil) and negative for a myopic eye (more light in the bottom of the pupil). The technique can be calibrated with trial lenses. The slope of the brightness profile is linearly related to refractive error, and the technique is ready for use once the conversion factor from slope to refractive error has been empirically established. Since the pupil is continuously tracked, alignment is not critical. A detailed description of the scanner version of the PR can be found elsewhere [21]. It also uses near-infrared light and the subjects' head movements are restricted by a chin rest. While the camera is located in a fixed location, a hot mirror is moving linearly in front of the subject each time compensating for the difference in angle between the eye and the camera with a rotational movement. The central 90 deg of visual angle are measured, sampling with a resolution of 0.6 deg. One scan takes about 4 s. When refraction along the horizontal and vertical pupil meridian is acquired, the mean spherical equivalent can be estimated as the average of both. While the HS scanner provides all the wavefront data at every measured point, the PR system only resolves defocus. Figure 1 shows pictures and schematic diagrams of both systems.

A. Subjects
The right eyes of 35 subjects were measured with both instruments under similar conditions. The measurements were done noncycloplegically under dim room illumination (<5 lux). Both instruments were located in the same room at the Laboratorio de Optica in Murcia, Spain, and the subjects were measured within 15 min in random order. In both cases, the fixation target was a distant point (2 m) on the wall that was seen with both eyes.

Students and employees of the Universidad de Murcia, with no known ocular pathology other than refractive errors, served as volunteer subjects. They were divided into two groups, emmetropic [mean $M \pm$ standard deviation (std)/ #subjects, -0.2 ± 0.5 D/22) (EMM) ($M \geq -0.75$ D)] and myopic [(-2.0 ± 0.9 D/11) (MYOP) ($M < -0.75$ D)]. The two
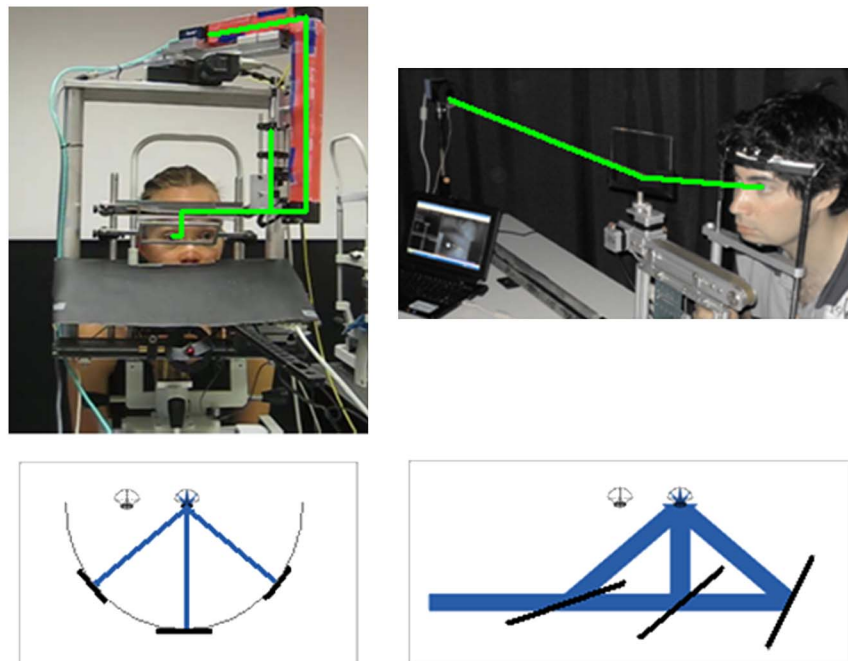

Fig. 1. (Color online) (Left) Photo and schematic of scanning principle of the HS scanner. (Right) Same as left, but for the PR scanner.

hyperopic subjects $(2.5 \pm 1.4 \; D/2)$ were pooled with the EMM group.

The use of the sensors and the experiment followed the tenets of the Declaration of Helsinki. All subjects were fully informed before participating in the study.

B. Data Analysis

To compare the performance of both devices, the mean spherical equivalent (M) was used. For the HS sensor, M was calculated from the Zernike coefficients of a 4 mm pupil diameter using only the second-order term. In the case of the PR system, M was calculated as the mean of the refractions along the horizontal and the vertical pupil meridian at each measured angle. The results of the measurements were used without recalculating them to a visible reference wavelength to prevent incorrect conversion [24]. Data from the central 80 deg of the visual field were compared. To ensure that the data originated from the same angular positions, the centers of the optic discs were aligned for both data sets. The angular sampling grid of the HS scanner was used as reference. Since the PR scanner sampled slightly denser, the averages of the refractions in the respective range were used. Measurements in the range of the optic disc ($8°–18°$ in the nasal retina) were not included in the comparisons due to high variability, possibly because the fundus reflectivity was variable in the optic disc area. Visual angles are expressed in degrees, using negative values for the temporal retina and positive values for the nasal retina.

Comparisons between the two devices involved scatterplots and Bland–Altman plots, including all raw data (except from the optic disc area). In addition we tested one situation where the data were recalculated using the regression function. A repeated measures analysis of variance (RM ANOVA) test was used to test if the measurements were significantly different over the whole visual range, and a paired t test for each angle was used to determine at which eccentricities significant differences occurred.

The mean relative peripheral refractive error (M RPRE) metric was calculated for each individual using the acquired data. The M RPRE metric is the mean of the relative refraction measured at each eccentricity leaving out the optic disc area. A negative M RPRE value represents a profile with relatively more peripheral myopic defocus. According to Rempt *et al.* [2], the M RPRE is more negative for emmetropes compared to myopes. The difference in M RPRE calculated from the HS data and the PR data were calculated and tested for all individuals using the Pearson correlation coefficient.

Finally, peripheral refraction profiles were analyzed by fitting polynomials. The order was increased until the root-mean-square (RMS) error of the fit was below a threshold value. An RM ANOVA test was used to examine if the best-fitting orders were similar for both instruments.

3. RESULTS

Figure 2 shows all data collected with the PR scanner compared with those data collected with the HS scanner. The R-square of the fitted regression line was 0.647 ($p < 0.001$). However, the slopes were not close to 1, nor were the offsets close to zero, which should be expected if both devices would measure the same values. Instead, the following regression equations were obtained: $M_{PR} = 1.421 \times M_{HS} + 0.513$ or $M_{HS} = 0.455 \times M_{RP} - 0.508$.
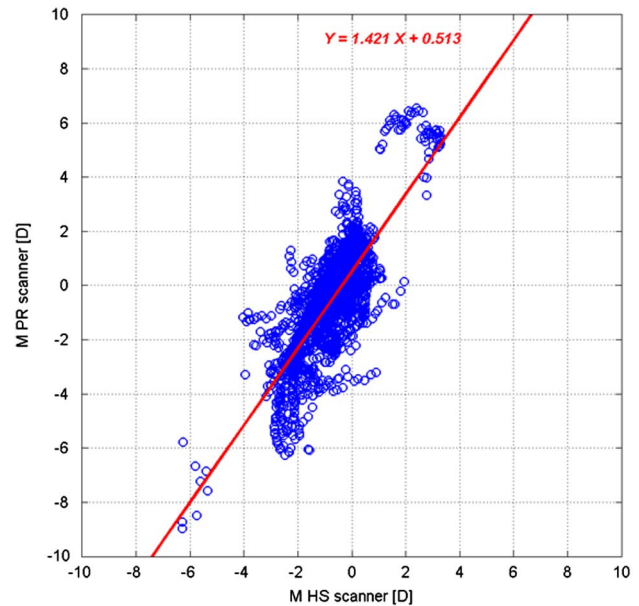

Fig. 2. (Color online) Refractions determined with the PR scanner (ordinate) plotted against the measurements with the HS scanner measurements (abscissa) from all subjects and at all angular positions ($n = 1965$ data points). Only data from the optic disc area are excluded.

Figure 3, left panel, shows the means and standard deviations of the measurements in the complete population for both instruments. Using an RM ANOVA test on the raw data, it was found that the data acquired with both instruments were significantly different ($p < 0.001$). Since Fig. 2 did not show a regression with a slope close to 1 and an offset close to zero, the PR data were, in a second step, adjusted using the linear regression equation $M_{PR} = 1.421 \times M_{HS} + 0.513$ such that these two conditions were satisfied. After conversion, the data from both devices were no longer significantly different in an RM ANOVA test ($p = 0.732$). The converted data are shown in Fig. 3, right panel.

As *post hoc* analysis, the difference of M measured with both instruments was tested with an RM ANOVA test for each angle separately. Significant differences (p-values <0.05) were found only between $22°$ to $35°$ in the nasal retina. As explained in the Methods section, the angular positions were matched, using the optic disc position in the eyes as reference, for each subject separately. Because of the lack of data in a major fraction of the subjects for angles above $+35°$, those data were no longer considered reliable and therefore omitted from the analysis.

When the mean refractions for the EMM subjects ($n = 21$) and the MYOP subjects ($n = 12$) were separately analyzed, it showed that emmetropes were slightly more hyperopic when measured with photorefraction than with the HS technique. The opposite was observed for the MYOP subjects (Fig. 4). The peripheral refraction profiles, however, had similar shapes with both techniques for the EMM group but deviated for the MYOP group, mainly in the temporal retina. A paired t test showed significant differences between the two instruments in the nasal retina but not in the temporal retina. For the emmetropes, this occurred at visual angles in the nasal retina above $+20°$, while, for the myopes, differences were detected also in the temporal retina below $-22°$.
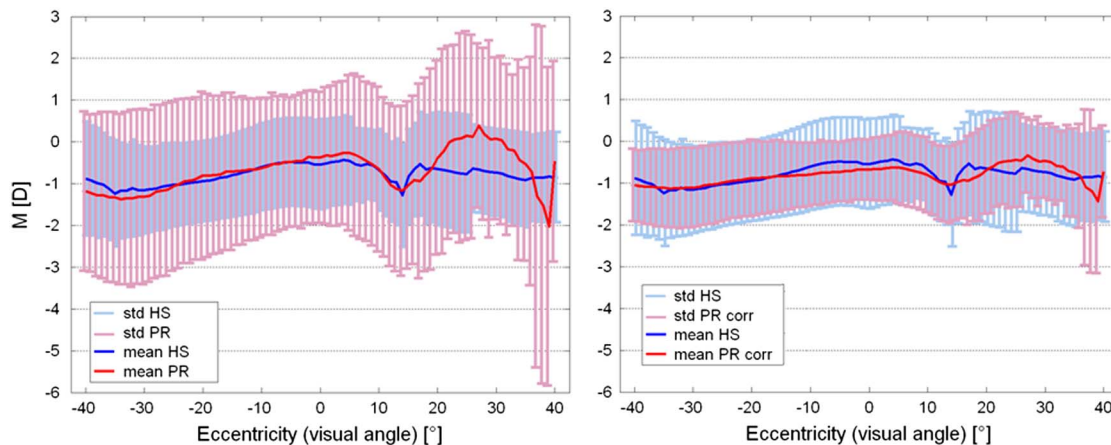
Fig. 3. (Color online) The left graph shows the mean and standard deviation of m as measured with the HS scanner and the PR scanner (raw data). The graph on the right shows the same data after correcting the data from PR scanner according to the regression equation $M_{PR} = 1.421 \times M_{HS} + 0.513$ as determined in Fig. 2.

Bland–Altman plots of the raw data and of the data corrected by the linear regression (see Fig. 3) are shown in Fig. 5. For the raw data, the mean difference was –0.19 D, and the 95% limit of agreement was quite large (–2.44 D).

A significant difference ($p = 0.001$) was found for the M RPRE between the EMM group (M RPRE = -0.48 ± 0.39 D) and the MYOP group (M RPRE = 0.14 ± 0.61 D) using the data measured with the HS scanner (mean and standard deviation are shown in the left plot of Fig. 6 along the horizontal axis, in blue the EMM and in red the MYOP). However, no significant difference ($p = 0.373$) was found in M RPRE between emmetropes (M RPRE = -0.19 ± 0.38 D) and myopes (M RPRE = -0.38 ± 0.89 D) for the PR scanner data (mean and standard deviation are shown in the left plot of Fig. 6 along the vertical axis, in blue the EMM and in red the MYOP). The mean of the M RPRE metric measured with the HS scanner for the EMM subjects was slightly higher than the mean of the M RPRE measured with the PR scanner (center of blue cross lays on the left of the 45° line in the left plot of Fig. 6), while the opposite was true for the MYOP subjects (the center of red cross in the left plot in Fig. 6 is on the right of the 45° line). The plot on the right in Fig. 6 shows the differences between the M RPRE data from both instruments for all subjects.
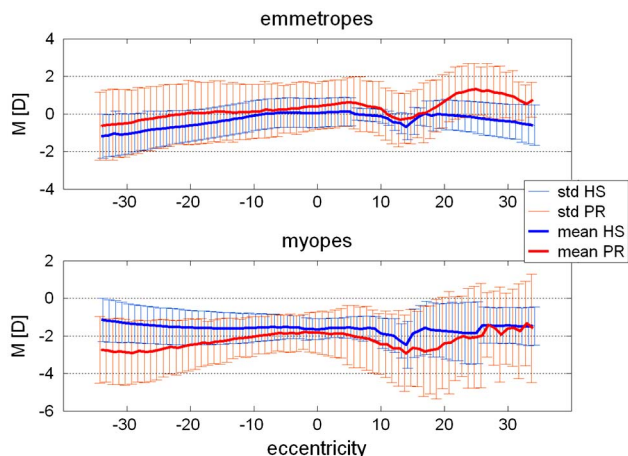
To examine the correlation of the measurements in more detail, Pearson correlation coefficients were calculated for the HS data versus the PR data for each individual separately. Large variation between individuals was found: the values ranged between 0.956 and −0.501 (mean ± std, 0.519 ± 0.403). Figure 7 shows the comparison between the HS data and PR data for two individuals taken at both extremes.

Finally, polynomials were fitted to M as a function of eccentricity. The order of the polynomial was increased until the RMS error of the fit was below a threshold of 0.2 D for the HS data. Because on average the measured M was larger for the PR measurements, the threshold value for the PR data fittings was increased with the ratio of the RMS of all PR data to the RMS of all HS data. Therefore, the threshold for the PR data was set at 0.3 D. The maximum fitted order was 6. An RM ANOVA test gave a p-value of 0.003, finding a mean order (std) of 2.5 (± 1.2) for the HS scanner and 3.6 (± 1.9) for the PR scanner.

4. DISCUSSION

The results provided by the scanning peripheral PR and HS sensor correlated moderately when the average data were compared. When individual correlations at any eccentricity angle were analyzed, correlations were still found, although with a poor identity relationship. In general, the PR scanner measured higher refraction values than the HS scanner. This could also be observed in the average refraction of the EMM and MYOP subjects. The values measured with the PR scanner were slightly higher than those measured with the HS scanner for the emmetropes, while the opposite situation occurred for the MYOP subjects. Both of those observations could be due to an artifact of calibration. The HS sensor is in this sense robust and only slightly dependent on calibration. In general linearity is found for the central refractions of the dynamic range of the sensor in which most measurements were taken. The PR technique relies strongly on calibration since the slope of the intensity profile is empirically related to the refraction. Variation in reflectivity of the measured retinal area, variation in intraocular scatter, higher-order aberrations, and corneal reflections are some parameters that could cause artifacts affecting the measurements. The optimal method for calibrating the PR scanner is still under investigation. To examine if the
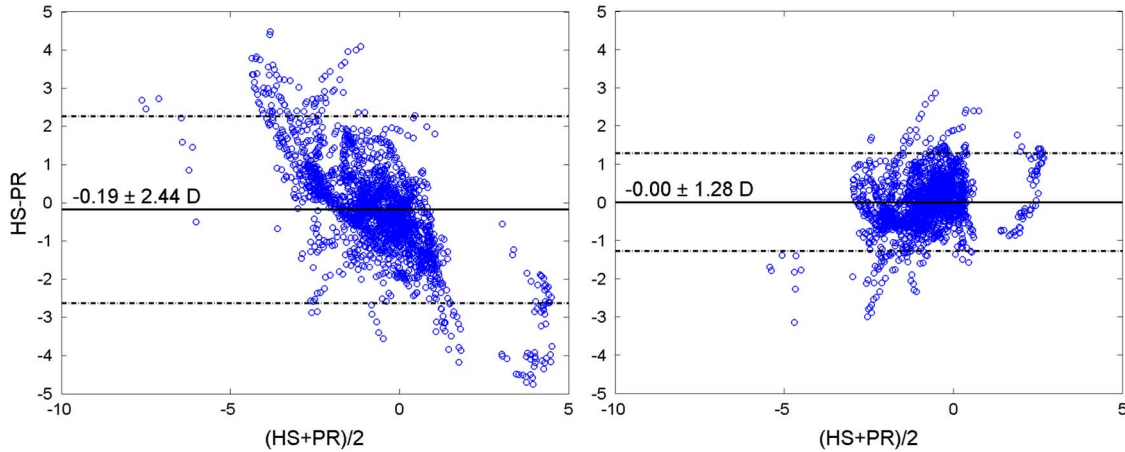

Fig. 4. (Color online) Means and standard deviations of the HS data and PR data for (top) the EMM subjects and (bottom) MYOP subjects.

Fig. 5.   (Color online) Bland–Altman plots for M, as measured with the HS scanner and the PR scanner, using (left) raw data and (right) data that were corrected with a linear regression.

observed differences between the two instruments could be due to a calibration error, the data of the peripheral PR were recalculated with respect to the HS scanner data using the correlation curve data. Afterward, no significant difference was found between the data measured with the HS scanner and the PR scanner. This reinforces the belief that the difference resulted from inadequate calibration presumable of the PR scanner

Although the PR technique only estimates refractive error, no correlation (0.042) was found between the size of the difference in M measured with both instruments and the higher-order RMS, calculated from the third- and fourth-order coefficients measured with the HS scanner, or with astigmatism (-0.071).

Potential future users should be advised that, although there is some correlation in the retrieved measurements, for some particular cases, the discrepancies can be very large. This can be noted in the right panel of Fig. 7.

A. Elliptic Pupil and Angular Dependency
With increasing eccentricity the pupil becomes elliptic. Because both instruments are based on totally different meth-

ods, they are also dealing differently with this problem. The HS scanner for off-axis measurements uses all measured HS spots to calculate the wavefront ("LC-method" according to [25]). The Zernike coefficients are initially determined for a unit circle including all measured spots. Then they are rescaled to a 4 mm circular pupil that falls fully within the area of the measured spots. Therefore, the result is not influenced by the earlier extrapolated area of the wavefront [25]. The impact of change of the center of the pupil plane when going off-axis could perhaps be a source introducing some error in the determination of the Zernike coefficients [18]. Nevertheless, the absolute impact has not been quantified. In case of the PR scanner, the measurements along the vertical pupil meridian are not influenced because the measurements were done along the horizontal visual axis. The refraction along the horizontal pupil meridian is suffering from decrease of the pupil diameter along this meridian. A correction factor was developed to compensate for this artifact.

From Fig. 4 it can be seen that the difference between the two instruments in general increases with eccentricity. When for each angle the mean difference of M between both instruments was calculated for the raw data and the converted data,
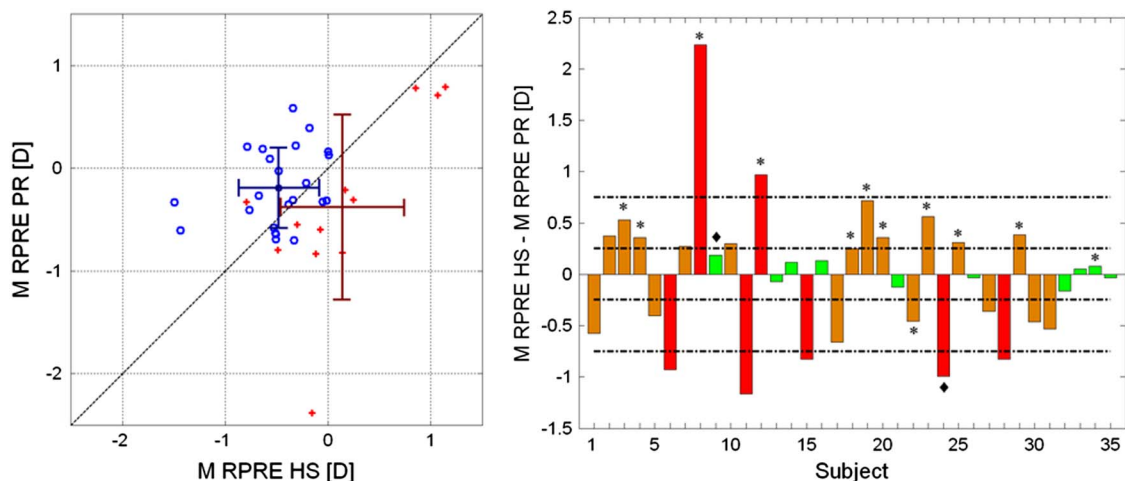

Fig. 6.   (Color online) The left plot represents a correlation plot of the M RPRE calculated from the HS data versus those calculated from the PR data. Also, the mean and standard deviation are given. Blue represents the EMM subjects and red the MYOP subjects. The right plot gives the difference between the M RPRE calculated from both instrument data for each of the subjects. The stars indicate the MYOP subjects; the subjects with the diamond (hyperopic) or no symbol represent the EMM group.
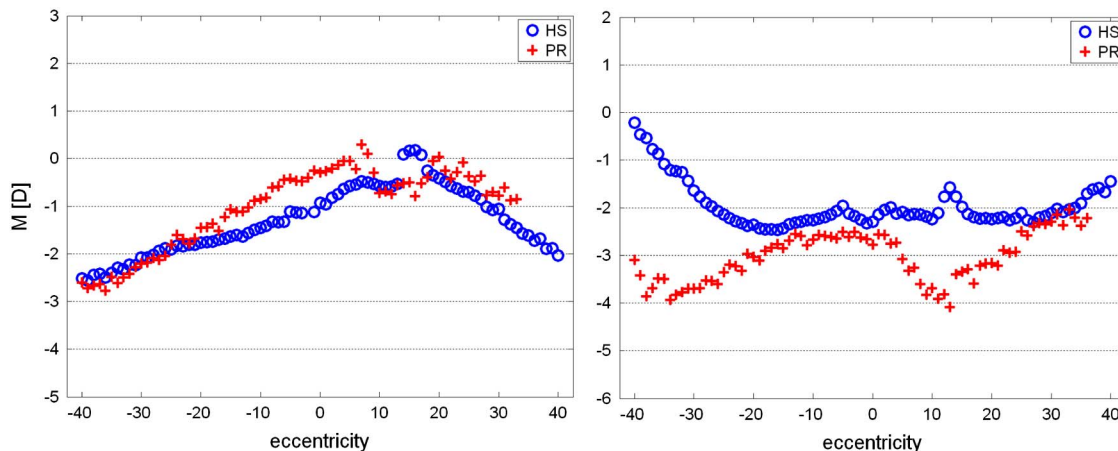
Fig. 7.　(Color online) The graph on the left shows measurements of both instruments in subject 25, representing a high correlation of the data ($R = 0.956$). On the right, data are shown from subject 23, in whom even a negative correlation ($R = -0.501$) was found.

an increase in the difference with eccentricity was found in both cases.

For the M RPRE, which is influenced strongly by the peripheral refraction, different trends were measured by the instruments. Especially for the MYOP subjects, the relative peripheral hyperopic refraction found with the HS scanner was converted to a relative peripheral myopic refraction.

The shape of M as a function of eccentricity fluctuates more for the PR data than observed for the HS data. On average, a higher-order polynomial was required to represent the shape of the peripheral refraction data measured with the PR scanner. Because the PR technique is based on relative variation in intensity over a pupil meridian, it could be influenced by variation of the reflectivity of the fundus or transparency of the optics of the eye (scatter) between different eccentricities. Also, the presence of corneal reflections or Purkinje images could disturb the determination of the correct slope. The HS technique is more robust in this matter as long as the center of the spots can be detected correctly. Iterative unwrapping algorithms can work around minor reflections distorting part of the spot pattern [26].

B. Illumination Difference

Observing the shape of the average refraction line (left image of Fig. 3) in the nasal retina, a strong deviation between the two instruments can be observed. From the statistical analysis, the mean refraction measured with the HS scanner and with the PR scanner was significantly different for the region between 22° and 35° of the nasal retina. Another observation from the mean refraction curves was that the size of the optic disk was different for both instruments. While the HS scanner measured a smaller diameter and steeper flanks, the PR scanner measured a slightly wider pit with flatter rims. It is speculated that the origin lies in the type of illumination. The illumination light of the HS scanner is a small (1 mm) collimated laser beam. The spot size on the retina will also be small and reasonable independent of the refractive errors or aberrations of the eye. The illumination of the PR scanner is an LED array at a large distance that fills the whole pupil. The illuminated area at retinal level is expected to be larger especially when the eye has a refractive error. Also, the increase of aberrations with pupil diameter will have its impact. When a larger area of the retina is illuminated, the result will be influ-

enced by an integration effect. The measured shape of the optic disk could be expected to be a convolution of the effective shape of the optic disc area and the illumination spot on the retina. The small differences in the illumination wavelength in the two instruments (780 versus 875 nm) should add a possible defocus shift of less than 0.15 D [27].

C. Pros and Cons of Both Instruments

Both tested instruments are the prototype versions (Fig. 1). Other things they have in common are that they are both reasonable compact systems operated with a conventional laptop. They measure optical properties of the human eye over a large angular range and with high angular resolution. When examining peripheral vision, both instruments provide more comfort for subject and operator. Nevertheless, the instruments are also very different and have therefore their own pros and cons.

The PR scanner is easy to align, consists of low-cost components, and the information on the measured pupil meridian is available in real time. Some drawbacks concern the moving mirror in front of the subject, the limited amount of available data, and the dependency of calibration and correction factors. The moving mirror in front of the subject is a hot mirror that is transparent for visible light and provides an open field of view, though it moves close to the subject who could be distracted. To reach the maximum scanning speed, only a limited amount of data is saved. A custom designed C++ program only saves the refraction along the measured pupil meridian, the pupil size along the measured pupil meridian, and a brightness metric. The impact and correction of various artifacts such as the change in pupil shape with eccentricity, the varying distance between the sensor and the eye while scanning, the variation of scatter at different angles, the difference of reflectivity of the fundus, the corneal reflections, and higher-order aberrations need to be optimized.

The advantages of the HS scanner are the open field of view without moving elements in the line of sight of the subject and the availability of the whole wavefront data from each measured angle. So the HS scanner provides a full description of the optical properties at every visual angle. All HS images are saved; therefore, the operator has the opportunity to do extensive postprocessing and analysis. The drawbacks of the HS scanner are the alignment time, the processing time,

and the higher cost (compared now to the PR scanner). Aligning the HS scanner to the subject is a little bit more laborious. For an experienced operator, it takes about 1 to 2 min to align a normal subject. This could also be beneficial because it gives the subject some time to get used to the instrument. The current version of the HS scanner consists of several costly components such as the high accuracy motor, an intensity-tunable 780 nm laser source, and a fast acquisition complementary metal oxide semiconductor camera. More optical components compared to the PR scanner are required, but all of them, except for the large fixed mirror (see [20]), are off-the-shelf components. The last drawback is the processing time. The operator has instantaneous availability to the HS spot images from which he will have to judge if the data acquisition was successful because the current software needs about 6 min to elaborate one scan (324 images). The final advantage of the HS scanner is that it probably provides more reliable data for a larger variety of eyes and measurement conditions.

5. CONCLUSIONS

Two prototype peripheral optics scanners were compared in 35 subjects. Comparing the average data, a correlation was found between both instruments, although with poor identity. This could have been caused by initial calibration errors in the PR system. Only for the range of 22° to 35° on the nasal retina were the mean refraction measured with the HS scanner and with the PR scanner found significantly different. The optic nerve measured with the PR scanner was slightly larger with flatter rims compared to the measurements with the HS scanner. However, a reasonable correlation was found for the mean data; the comparison for each subject individually varied strongly. The M RPRE was found to be significantly different between EMM and MYOP subjects when calculated from the HS data, while it was not significantly different when calculated from the PR data. In general the shape of the peripheral refraction varied more with eccentricity when measured with the PR scanner than when it was measured with the HS scanner. A thoroughgoing investigation on the error sources of both instruments will be necessary to get a better understanding of the differences and for the development of a gold standard for measuring peripheral image quality.

ACKNOWLEDGMENTS

REFERENCES

1. J. Hoogerheide, F. Rempt, and W. P. H. Hoogenboom, "Acquired myopia in young pilots," Ophthalmologica **163**, 209–215 (1971).
2. F. Rempt, J. Hoogerheide, and W. P. H. Hoogenboom, "Peripheral retinoscopy and skiagram," Ophthalmologica **162**, 1–10 (1971).
3. J. Wallman, M. D. Gottlieb, V. Rajaram, and L. A. Fugate-Wentzek, "Local retinal regions control local eye growth and myopia," Science **237**, 73–77 (1987).
4. A. Seidemann, F. Schaeffel, A. Guirao, N. Lopez-Gil, and P. Artal, "Peripheral refractive errors in myopic, emmetropic, and hyperopic young subjects," J. Opt. Soc. Am. A **19**, 2363–2373 (2002).
5. J. Wallman and J. Winawer, "Homeostasis of eye growth and the question of myopia," Neuron **43**, 447–468 (2004).
6. E. L. Smith, L. Hung, and J. Huang, "Relative peripheral hyperopic defocus alters central refractive development in infant monkeys," Vis. Res. **49**, 2389–2392 (2009).
7. E. L. Smith, L. Hung, J. Huang, T. L. Blasdel, T. L. Humbird, and K. H. Bockhorst, "Effects of optical defocus on refractive development in monkeys: evidence for local, regionally selective mechanisms," Investig. Ophthalmol. Vis. Sci. **51**, 3864–3873 (2010).
8. E. L. Smith, R. Ramamirtham, Y. Qiao-Grider, L. Hung, J. Huang, C. Kee, D. Coats, and E. Paysse, "Effects of foveal ablation on emmetropization and form-deprivation myopia," Investig. Ophthalmol. Vis. Sci. **48**, 3914–3922 (2007).
9. M. Millodot, "Effect of ametropia on peripheral refraction," Am. J. Optom. Physiol. Opt. **58**, 691–695 (1981).
10. D. O. Mutti, J. R. Hayes, G. L. Mitchell, L. A. Jones, M. L. Moeschberger, S. A. Gotter, R. N. Kleinstein, R. E. Manny, J. D. Twelker, and K. Zadnik, "Refractive error, axial length, and relative peripheral refractive error before and after the onset of myopia," Investig. Ophthalmol. Vis. Sci. **48**, 2510–2519 (2007).
11. J. Tabernero and F. Schaeffel, "More irregular eye shape in low myopia than in emmetropia," Investig. Ophthalmol. Vis. Sci. **50**, 4516–4522 (2009).
12. J. Tabernero, D. Vazquez, A. Seidemann, D. Uttenweiler, and F. Schaeffel, "Effects of myopic spectacle correction and radial refractive gradient spectacles on peripheral refraction," Vis. Res. **49**, 2176–2186 (2009).
13. P. Sankaridurg, L. Donovan, S. Varnas, A. Ho, X. Chen, A. Martinez, S. Fisher, Z. Lin, E. L. Smith, J. Ge, and B. Holden, "Spectacle lenses designed to reduce progression of myopia: 12-month results," Optom. Vis. Sci. **87**, 631–641 (2010).
14. L. Lundström, A. Mira-Agudelo, and P. Artal, "Peripheral optical errors and their change with accommodation differ between emmetropic and myopic eyes," J. Vision **9**, 17 (2009).
15. W. N. Charman and H. Radhakrishnan, "Peripheral refraction and the development of refractive error: a review," Ophthalmic Physiolog. Opt. **30**, 321–338 (2010).
16. H. Radhakrishnan and N. Charman, "Peripheral refraction measurement: does it matter if one turns the eye or the head?" Ophthalmic Physiolog. Opt. **28**, 73–82 (2008).
17. P. Prado, J. Arines, S. Bará, S. Manzanera, A. Mira-Agudelo, and P. Artal, "Changes of ocular aberrations with gaze," Ophthalmic Physiolog. Opt. **29**, 264–271 (2009).
18. C. Fedtke, F. Manns, and A. Ho, "The entrance pupil of the human eye: a three-dimensional model as a function of viewing angle," Opt. Express **18**, 22364–22376 (2010).
19. C. Fedtke, K. Ehrmann, and B. A. Holden, "A review of peripheral refraction techniques," Optom. Vis. Sci. **86**, 429–446 (2009).
20. B. Jaeken, L. Lundström, and P. Artal, "Fast scanning peripheral wave-front sensor for the human eye," Opt. Express **19**, 7903–7913 (2011).
21. J. Tabernero and F. Schaeffel, "Fast scanning photoretinoscope for measuring peripheral refraction as a function of accommodation," J. Opt. Soc. Am. A **26**, 2206–2210 (2009).
22. P. M. Prieto, F. Vargas-Martin, S. Goelz, and P. Artal, "Analysis of the performance of the Hartmann–Shack sensor in the human eye," J. Opt. Soc. Am. A **17**, 1388–1398 (2000).
23. F. Schaeffel, L. Farkas, and H. C. Howland, "Infrared photoretinoscope," Appl. Opt. **26**, 1505–1509 (1987).
24. B. Jaeken, L. Lundström, and P. Artal, "Peripheral aberrations in the human eye for different wavelengths: off-axis chromatic aberration," J. Opt. Soc. Am. A **28**, 1871–1879 (2011).
25. L. Lundström, J. Gustafsson, and P. Unsbo, "Population distribution of wavefront aberrations in the peripheral human eye," J. Opt. Soc. Am. A **26**, 2192–2198 (2009).
26. L. Lundström and P. Unsbo, "Unwrapping Hartmann–Shack images from highly aberrated eyes using an iterative B-spline based extrapolation method," Optom. Vis. Sci. **81**, 383–388 (2004).
27. E. J. Fernández and P. Artal, "Ocular aberrations up to the infrared range: from 632.8 to 1070 nm," Opt. Express **16**, 21199–21208 (2008).